Article

Mapping of Alpha-Emitting Radionuclides in the Environment Using an Unmanned Aircraft System

Pablo Royo [*] , Arturo Vargas , Tania Guillot , David Saiz , Jonathan Pichel , Daniel Rabago , María Amor Duch , Claudia Grossi , Maksym Luchkov , Volker Dangendorf , Faton Krasniqi

Article

Mapping of Alpha-Emitting Radionuclides in the Environment Using an Unmanned Aircraft System

Pablo Royo [1,*,†]**, Arturo Vargas** [2,†]**, Tania Guillot** [1,†]**, David Saiz** [1,†]**, Jonathan Pichel** [1,†]**,
Daniel Rabago** [3,†]**, María Amor Duch** [2,†]**, Claudia Grossi** [2,4,†]**, Maksym Luchkov** [5,†]**,
Volker Dangendorf** [5,†] **and Faton Krasniqi** [5,†]

[1] Castelldefels School of Telecommunications and Aerospace Engineering—Technical University of Catalonia, 08860 Castelldefels, Spain; tania.guillot@upc.edu (T.G.); david.saiz.vazquez@upc.edu (D.S.); jonathan.pichel@upc.edu (J.P.)
[2] Institute of Energy Technologies (INTE)—Technical University of Catalonia, 08028 Barcelona, Spain; arturo.vargas@upc.edu (A.V.); maria.amor.duch@upc.edu (M.D.); claudia.grossi@upc.edu (C.G.)
[3] University of Cantabria (UC), Avd. Herrera Oria s/n 39011 Santander, Spain; daniel.rabago@unican.es
[4] Physic department, Technical University of Catalonia, 08028 Barcelona, Spain
[5] Physikalisch-Technische Bundesanstalt (PTB), 38116, Braunschweig, Germany; maksym.luchkov@ptb.de (M.K.); volker.dangendorf@ptb.de (V.D.); faton.krasniqi@ptb.de (F.K.)
* Correspondence: pablo.royo@upc.edu (P.R.); Tel.: +34-93-417108
† These authors contributed equally to this work.

Abstract: The protection of first responders from radioactive contamination of alpha emitters that may result from a radiological accident is of great complexity due to the short range of the alpha particle in air of a few cm. To overcome this issue, for the first time a system for near real-time measuring alpha particles remotely mounted on a UAS has been developed, tested and calibrated. The new system, based on an optical system adapted to be installed on the UAS in order to measure the UV-C fluorescent emitting by the alpha particle in air, has been tested and calibrated carried out by laboratory and in field experiments using UV-C leds and ^{241}Am sources. In experimental flights, the probability of detecting a point source was determined to be approximately 60%. In case of a surface extended source, a detection efficiency per unit surface activity of ten counts per second per MBq cm^{-2} are calculated. A background count rate of UV-C around 26 ± 28 s^{-1} for an integration time of 0.1 s was measured during flights, which leads to a decision threshold surface activity of 5 MBq cm^{-2}.

Keywords: UAS; radiological detection; alpha-emitting radionuclides; UAS software architecture

1. Introduction

The protection of first responders and the general public against radioactive contaminations caused by accidental or deliberate radiological events, including terrorist attacks and a possible war scenario, is critical. After a nuclear or radiological accident event, the decision-makers must understand the spread of contamination and the affected area. This information is crucial to determine the most suitable response. In the immediate vicinity of a nuclear or radiological event, or in case of large-area ground contaminations, the remote detection of alpha and gamma radioactivity by using Unmanned Aircraft Systems (UAS) is an excellent solution to assess the contaminated area before the first responders enter in order to protect them against contamination and irradiation.

In the event of such type of radiological or nuclear area contamination, the decay of the present radionuclides in the scenario can emit alpha, beta particles and gamma-rays. Most of the potential radionuclides inventory in this type of accidents emits gamma-rays of different energies, which have a long-range distance that can reach hundreds of meters, before its energy is completely absorbed and therefore, can be measured remotely. On the other hand, if alpha-emitter radionuclides are preset

in the accident, their remote detection is much more complicated because the very short range in air of only a few centimeters.

In the case of contaminations with gamma-emitting radionuclides, spectrometric gamma detectors that can both, identify radionuclides and deduce the dose rate such as scintillators or semiconductors detectors, have already been mounted on the UAS and are commercially available. The characterization of the response of spectrometric gamma detectors mounted on UAS have been carried out in different works as in the framework of the European project "Preparedness"[1] [1,2].

In case of a radiological scenario involving the dispersion of alpha-emitting radionuclides in the environment, the situation is significantly more complicated. In addition to its short range distance, ingestion or inhalation of alpha-emitting radionuclides leads to a higher associated health risk compared to gamma-emitting sources for the same intake. Alpha particles deposit all their energy in a relatively short path, usually resulting in double-strand deoxyribonucleic acid (DNA) breaks that are difficult to repair unlike single-strand DNA breaks caused by gamma-rays. [3,4].

A detection system to remotely measure alpha particles is not commercially available and, currently, in order to minimize the health risk in an event with this kind of radionuclides, it is necessary to provide the first responders with appropriate protection equipment and with alpha detectors that should be located very close to the alpha-emitter radionuclide. This lead to highly time consuming and tedious task. Optical detection of alpha particle emitters is a technique that could be an interesting solution to measure remotely the alpha-emitters radionuclides and avoid to put the personnel at risk.

The physical principle of the optical technique is based on the alpha radiation detection via radioluminescence of air. Alpha particle induces radioluminescence light when absorbed in air. Radioluminescence in air is generated mostly by the emission of molecular nitrogen (N_2), and to a much lesser extent, by trace amounts of nitric oxide (NO) in air, with wavelength spanning three ultraviolet (UV) bands and about 99% of emission occurring in the 280 – 440 nm spectral range [5–7]. The diurnal background light is composed of approximately 95% UV-A (wavelengths from about 315 nm to 400 nm), 5% UV-B (wavelengths from about 280 nm to 315 nm), and almost no UV-C (wavelengths from about 100 nm to 280 nm). Therefore, the optical detection of alpha-emitting radionuclides is complex because the UV-A emissions are eclipsed by the much greater solar irradiance. Due to the low UV-C background emissions, the idea of acquiring only the UV-C (solar blind) light during daytime is a good alternative. However, the intensity of UV-C radioluminescence is very low (< 1%) which makes the detection quite challenging.

The alpha-induced air luminescence has been estimated to generate approximately 19 photons/MeV (at 1013 hPa, 22°C, and 43% relative humidity), and the dependence is found to be linear in the studied energy range from 0.3 MeV to 5.1 MeV [6]. The emitted photons are mainly in the UV-A wavelengths, and only about 0.2 photons/MeV belong in the UV-C wavelength range [7]. The radioluminescence signal is influenced by the characteristics of the gas atmosphere mainly due to the quenching effects of water vapor and oxygen. The UV-A photon yield can be increased by using a high-purity nitrogen atmosphere, whilst adding trace amounts of NO to the nitrogen atmosphere causes a sharp increase in the UV-C light yield. In the work of Kerst and Toivonen [8], the intensity of the UV-C signal was maximized at 50 ppm NO diluted in pure nitrogen. Also, this effect has been illustrated in the work of Krasniqi et al. [9] where activities as low as 300 Bq were measured in uranium samples using 3 ppm of NO.

The work presented in this paper has been developed within the framework of the European RemoteALPHA project. The RemoteALPHA project (2020-2023) [10] had the overall objective to develop novel optical systems and methodologies for the remote detection and quantification of large-scale contamination with alpha emitters in the outdoor environment, allowing sound and quick countermeasures in the case of a radiological emergency. One of the objectives was focused on the development of an unmanned airborne monitoring system (UAMS) which integrates the UAS with

---

[1] Preparedness: Metrology for mobile detection of ionising radiation following a nuclear or radiological incident (http://www.preparedness-empir.eu/)

a novel alpha-radioluminescence detection system to scan and obtain a map of the contaminated area in real-time. This paper focuses on the description of a novel developed system to measure remotely alpha-emitter radionuclides, mounted for the first time in an UAS, that would reduce significantly the risk to the first responders and to support decision-maker in case of a radiological or nuclear accident. To the authors' knowledge, this is the first time that alpha particles have been detected from a UAS. There are currently no commercial systems available to measure alpha particles remotely from a UAS. Section 2 details the materials and methods used to perform the UAS missions. This includes the hardware components, air-ground communications, and software architecture. Section 3 discusses the detector calibration results obtained both in laboratory conditions and during flight campaigns conducted at the Drone Research Laboratory (DroneLab) of the Technical University of Catalonia (UPC) [11]. Finally, Section 4 provides the main discussions and conclusions of this work.

2. Materials and Methods

This Section introduces the developed hardware and software to detect alpha-emitting radionuclides at a distance using an upgraded version of RIMA Software Architecture [1]. The different components of the developed system are presented including the optical detector, the UAS, radiological sources, the laser altimeter, air-ground communications, and the on-board computer. This Section also explains the calibration method used to characterize the light collection efficiency and field of view of the detector in a controlled laboratory environment using the UV sources that simulate the photon yield of alpha sources. At last, the software developed to send and display the alpha-emitting radionuclides in near real-time at the UAS Ground Control Station (GCS) is presented.

2.1. Hardware Architecture

This Section describes all the equipment used during the project to perform the alpha particle detection flights explaining the specific role of each instrument or sensor.

2.1.1. Detector

The initial step was to design and build an optical alpha detection system mountable on a commercial UAS. The detection of the light emitted by the radioluminescence resulting from the interaction of alpha particles with air comprises several phases. The first phase is to collect the emitted light (light collection), in an intermediate part the wavelength of interest (UV-C) must be filtered out (photon filtering), and finally the number of photons arriving at the detector must be counted (photon counting).

The radioluminescence light collection is done by a Polymethyl-methacrylate (PMMA) Fresnel lens with a diameter of 452.9 mm and a focal length of 424.5 mm chosen to ensure a high light throughput in a manageable form factor [12]. The photon filtering is done with 3 Semrock FF01-260/16-25 interference bandpass filters centered at 260 nm with a bandwidth of 16 nm. To achieve the best UV-C band filtering, a set of two corrective fused silica lenses (Thorlabs LC4252 and LA4052) was installed to parallelize the collimated photon beam. An additional filtering performance was achieved by tilting two filters in the set by 3 degrees relative to the optical axis.

The photon counting is done with a Photo Multiplier Tube (PMT) detector, that converts an incident light into an electrical signal analyzed by a digital pulse processing unit. The detection system uses the solar-blind Hamamatsu H11870-09 photomultiplier tube [13] with transistor-transistor logic (TTL) output and the GBS Elektronik MCA527 OEM+ multichannel analyzer [14] working in the scaler (gating) mode to translate these TTL signals into the timestamped count rate. During the flight, the count rate is polled and transmitted to the GCS to be displayed on a map for subsequent interpretation. If the count rate exceeds the threshold determined by the background rate, the source is present in the detector's field of view.

A carbon fiber-reinforced cone-shaped polymer frame has been built to hold the lens and the detection system. The frame materials were chosen to provide the necessary stability for the system while keeping it lightweight. The detector has a height of 790 mm and a diameter of 520 mm at the

base. Figure 1 shows an image of the detector and its different parts in a horizontal position during laboratory tests.
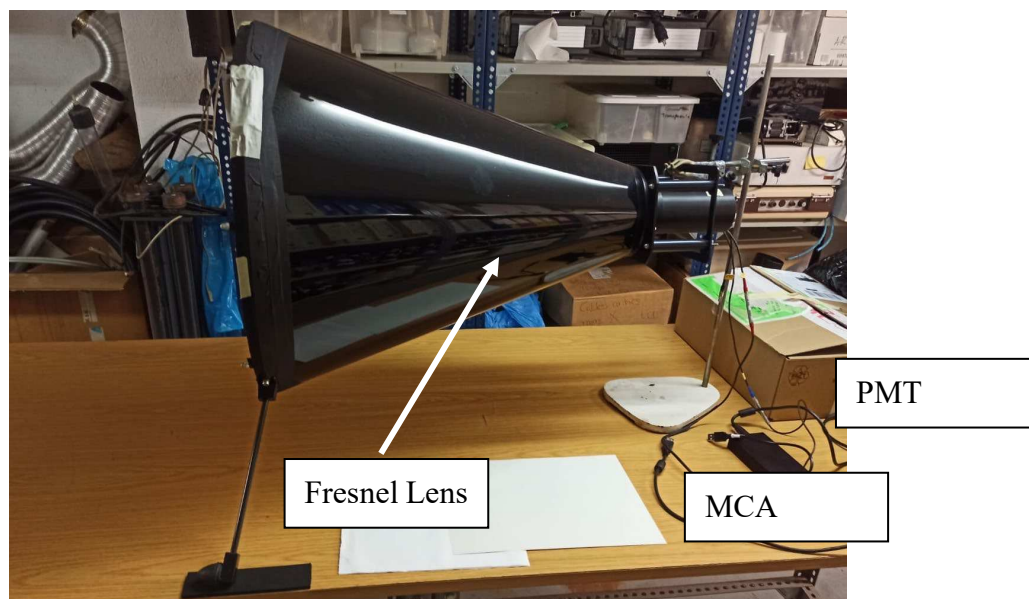

Figure 1. An optical system detector and its components developed for the measurement of alpha particles and optimised for mounting on an unmanned aircraft.

2.1.2. Characterization of the Detector

Investigation of the detector response was first performed under light-controlled conditions with UV LEDs to determine the field of view (FoV) and the best focusing configuration for the flights. In addition, the change in efficiency as a function of the angle of incidence and the power of the LED lamp was investigated. The results of these experiments are presented in Section 3.

The LED lamp used to test and optimize the optical system had a 5 mm thick Teflon disc at the exit aperture and was calibrated with a ^{210}Po activity standard. The LED lamp allows 12 different power modes, from number 0 to 11 (see Figure 2), simulating alpha sources with energy 5.4 MeV and activities up to 7.3 GBq (setting Nr. 11).
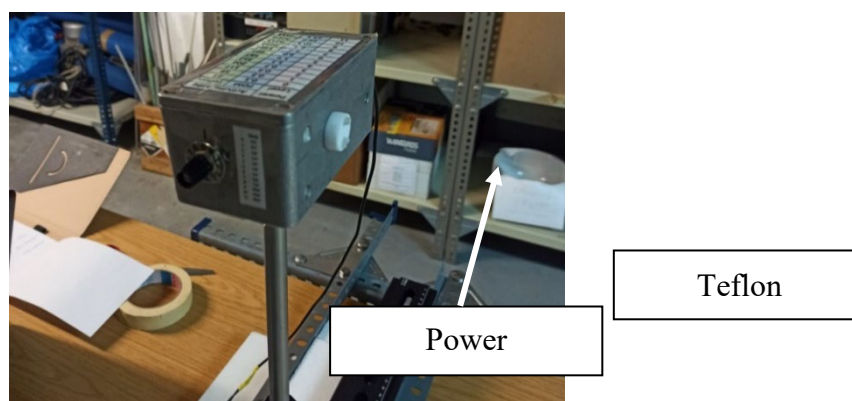

Figure 2. Calibrated UV-C LED lamp and its components used to test the optical system detector, get the focus configuration and the detector field of view.

The optical system has a sliding detector design which allows adjusting the focus according to the object distance. The efficiency of each focusing configuration, represented by detector position *F* (protrusion from the frame in centimeters) was tested with the LED source placed at the optical axis at various distances as illustrated in Figure 3.
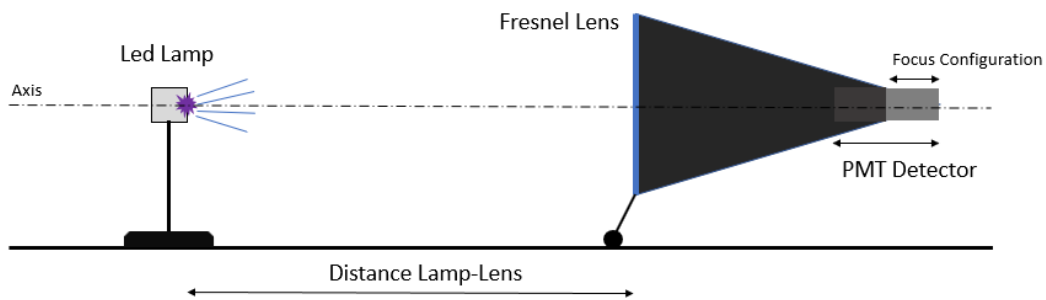
Figure 3. Scheme representation of the optical system focus configuration and field of view tests.

The field of view (FOV) is defined as the diameter of the spot that can be seen by the optical detection system. It depends on the focal length of the used receiving optics and the object distance. While in the simple lens-PMT case, the FOV can be estimated with a formula, the use of corrective lenses and non-trivial filter allocation required experimental evaluation. To determine the field of view, the LED source was moved perpendicularly to the optical axis.

The FOV is calculated by fitting the experimental data to a Gaussian function. The amplitude A and the standard deviation σ are calculated. The FOV is defined by the integral area in [-2σ, +2σ] range that implies ca. 95% of the total light collected.

The angular field of view (AFOV), the angle at which the detector can collect the light, is another important metric for drone-assisted optical measurements. It is calculated from the FOV and the distance between the object and the lens:

$$\text{AFOV} = 2 \cdot \text{atan}\left(\frac{\text{FOV}/2}{d}\right) \tag{1}$$

To assess how the tilt of the UAS can affect the light collection efficiency, the radio-luminescence signal has been measured as a function of the angle between the Fresnel lens optical axis and UV LED axis using a rotation platform with 1° precision.

This was the method used to calculate the field of view of the detector, the appropriate focus setting, and the count rate values provided by the LED source. Section 3 details the graphs obtained from these experiments in the laboratory.

2.1.3. Unmanned Aircraft System (UAS)

Given the dimensions of the detector (see Figure 4), no commercial UAS was high enough to natively integrate the detector under its belly, since the height of the detector is larger than UAS legs. This made it difficult to integrate the detector into a commercial UAS unless the detector itself acted as a landing gear. Therefore, four legs were attached to the detector so that the structure of the Fresnel lens is used as the landing gear of the unmanned aircraft. Figure 4 shows the Fresnel lens detector structure with a scheme of the landing legs and their dimensions.
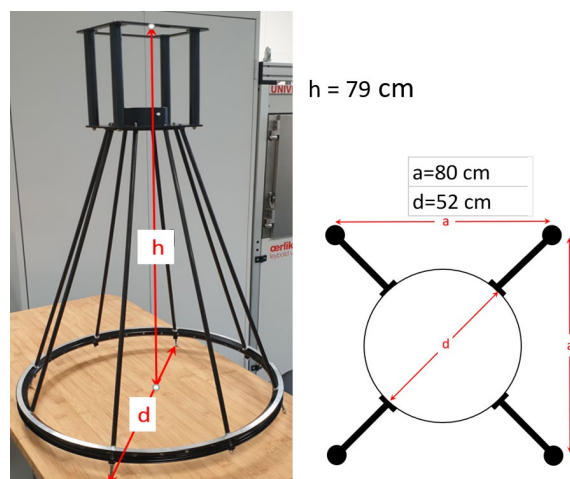
Figure 4. The optical system detector structure (**left**) and the landing legs add-on scheme (**right**).

Table 1 displays a summary of the weight of each UAS payload element and the sum of all components.

Table 1. Weight estimation of each component of the unmanned aircraft systems payload.

Components	Weight (grams)
Detector Structure and Landing Gear	2591
PMT detector	408
GBS MCA527OEM + onboard computer + air-ground communications and wires	468
TOTAL	3467

Two UAS from the Technical University of Catalonia (UPC) fleet were selected as possible candidates to mount the payload described in Table 1: DJI WIND 4 (W4) and DJI Matrice 600 Pro (M600P). Figure 5 shows pictures of both UAS. The authors have extensive experience with the M600P flight detector for radiological measurements, as it was used in previous projects such as "Preparedness" [1,2]. In addition, the M600P incorporates newer flight technology than the W4. For instance, the M600P is equipped with the A3 Pro flight controller, which improves control accuracy while increasing overall safety. On the other hand, the W4 has a better payload weight and flight autonomy than the M600P. However, the landing legs of W4 suffer from mechanical stress at high payloads. Another drawback of the W4 is the placement of the batteries, which would make integration of the detector into the UAS more difficult. Given the extensive operational experience, the improved avionics of the UAS, and easy payload integration, the M600P was chosen to mount the radioluminescence detector.

Figure 5. Unmanned Aircraft System candidates for mounting the alpha detector system.

Since M600P was not equipped with a Real-time Kinematic (RTK) system that greatly enhances the positioning accuracy, especially in the vertical profile, the Lightware SF11/C laser altimeter [15] was installed on the UAS. This altimeter has a long range (100 m), fast update rate (20 readings per second), and lightweight (35 g) laser designed specifically to be used on UAS. The M600P technical specifications provided by the manufacturer, without RTK, indicate that the UAS has a vertical flight accuracy of ±0.5 m, however the accuracy of the laser altimeter is 0.1 m.

2.1.4. Onboard Computer and Air-Ground Communications

Each measurement carried out with the optical detector must be geo-tagged during the flight for near real-time mapping. Taking this task, the onboard computer fuses UAS telemetry and the detector count rate data. The optical detector can provide a count rate measurement every 100 milliseconds. When the term "near real time" is used in this paper, it refers to the ability of the ground operator to observe in-flight measurements as they occur, without implying that the entire system responds within a specific fixed time frame. Typically, this time frame ranges from a few milliseconds to one or two seconds in worth cases with very low communication coverage. The system's response time variations do not affect the application's normal functioning and normal monitoring of the measurements taken.

The Raspberry Pi 4 Model B was chosen as the onboard computer [16]. This single-board computer is excellent for prototyping due to its low weight, large number of ports for connecting devices, and large support community. The Raspberry Pi 4 Model B has a Quad-core Cortex-A72 (ARM v8) 64-bit SoC with 1.8 GHz and 8 GB SRAM. The board also features 2.4 GHz and 5 GHz IEEE 802.11ac wireless LAN, Bluetooth 5.0, two USB 3.0 ports, two USB 2.0, Gigabit Ethernet, and an extended 40-pin General-Purpose Input/Output (GPIO) header where six UARTs can be found. Two of the six available ports are used. One of the UARTs is connected to the UAS autopilot to receive its telemetry and extract its current position and UAS attitude. The second UART port is used to connect the laser altimeter to obtain an accurate altitude.

The air-ground communication with the onboard computer is performed through Sixfab Raspberry Pi 4G/LTE Cellular Modem Kit [17]. The kit provides all the components for establishing an Internet connection on the Raspberry Pi. This allows interaction with the onboard computer at any given time, in near real time, and from anywhere in the world, as long as it is connected to the Internet. Through this connection, the geo-tagged measurements taken by the detector are sent to the ground control station.

The onboard computer and 4G/LTE air-ground communications are powered using the UAS batteries. The M600P has a connector that provides an 18 V - 7 A power output. The voltage must be converted to 5 V to power the onboard computer, for which the HOBBYWING regulator capable of providing 5 V and 3 A was used. Figure 6 shows the integration of the Raspberry PI, the 4G/LTE model with its corresponding antennas and the voltage regulator. It also shows the connection of the autopilot and the laser altimeter (right panel).
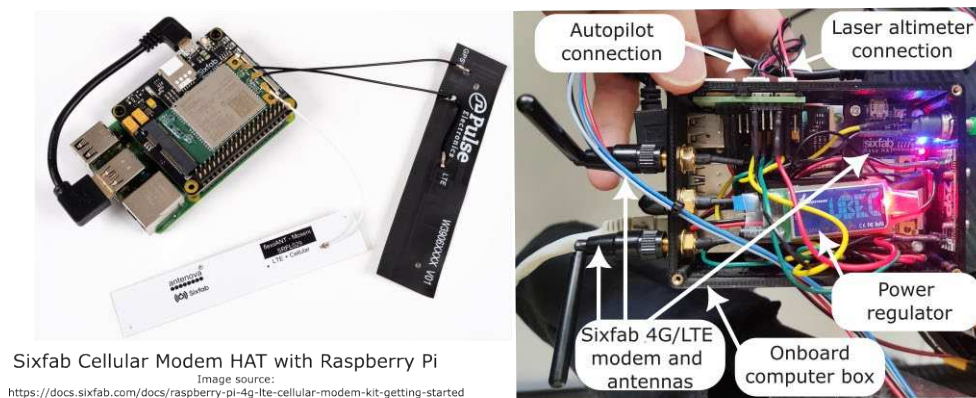
Figure 6. On the left, the cellular modem coupled to the on-board computer is illustrated. On the right, all components of the on-board computer are shown.

The system presented in this work is a first prototype. It has been assumed that 4G/LTE coverage will always be available to communicate with the UAS, in order to avoid adding more complexity. However, in the event of a nuclear catastrophe where the 4G/LTE network may not be available, an auxiliary point-to-point communication system that does not rely on the 4G/LTE network should be available. For instance, a radio modem system using the 868 MHz ISM band for Europe or the 900 MHz ISM band for the United States.

2.1.5. The Hardware Integration in the UAS

The alpha radioluminescence detector with the landing legs, the MCA counter, the laser altimeter, and the onboard computer with a 4G/LTE modem were integrated with the M600P as shown in Figure 7. The figure also displays the flat landing pad required for the takeoff and landing of the assembled UAMS due to the low clearance between the lens and the ground.

The following subsections describe the radiation and ultraviolet (UV) sources used during the test and validation flights.

Figure 7. Optical detection system integrated with the unmanned aircraft systems and ready to fly.

2.2. UV Sources

To verify the operation of the system, it is necessary to check it in conditions where alpha radiation sources or similar are present. The problem with using alpha radiation sources lies in the stringent radiation protection protocols for both the airfield and the transport to the test site, which limits the flexibility of outdoor testing. Although alpha sources were used during the final flights, in many preliminary tests they were replaced by LED sources that simulate the UV emitted by the air radioluminescence.

2.2.1. UV-C LED Sources

The UV-C LED sources used in the flights are commercially available and commonly used for water purification, disinfection, and sterilization of home aquariums. The LED has a peak wavelength between 270 nm and 280 nm and a radiant flux of 8 mW. Teflon sheets of a few millimeters are used to moderate the radiant flux to the level representative of radioactive sources that could be found in an emergency scenario. In addition, Teflon sheets serve to diffuse the light increasing its angular spread.

As per Section 3.1 results, the calculated FOV of the detector of only a few centimeters makes the detection of point sources significantly more complex than in the case of an extended source scenario. To analyze the detection probability of point sources, five LEDs were fabricated as shown in Figure 8. Therefore, five simulated alpha sources were distributed over the flight area to test the performance of the system in detecting the point sources.
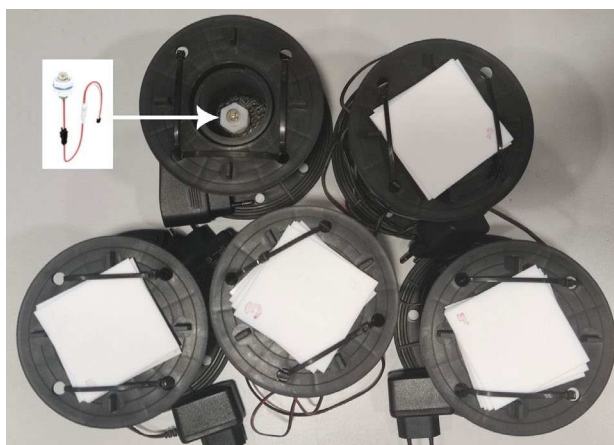

Figure 8. Five ultraviolet type CLEDs fabricated to simulate alpha sources with teflon sheets on top.

2.2.2. Americium Source

The reference alpha source used in the flights was manufactured by Eckert & Ziegler Cesio s.r.o (Czech Republic). The provided sealed foil of ^{241}Am source had an activity of 100 MBq (activity tolerance: + 0%, - 30%). ^{241}Am is an alpha and gamma emitter [18], with the most probable alpha emission at 5485.56 keV (84.45%) and the most probable gamma emission of 59.54 keV (35.92%).

According to the manufacturer, the ^{241}Am source consists of a thin AuPd layer where the ^{241}Am matrix of 1 μm thickness has been homogeneously incorporated. The source has an overall thickness of 0.25 mm consisting of a silver backing and a very thin layer of gold (< 2 μm thickness) covering the alpha-emitting face. The lateral dimensions of the foil are:

- Active dimensions: 20 mm x 100 mm.
- Overall dimensions: 30 mm x 100 mm.

To fulfil the radiation source handling requirements, the ^{241}Am foil was mounted on an aluminum base plate and covered with a quartz dome optically transparent to the radioluminescence produced by alpha particles in the air (see Figure 9 and Figure 10). The chamber design allows it to

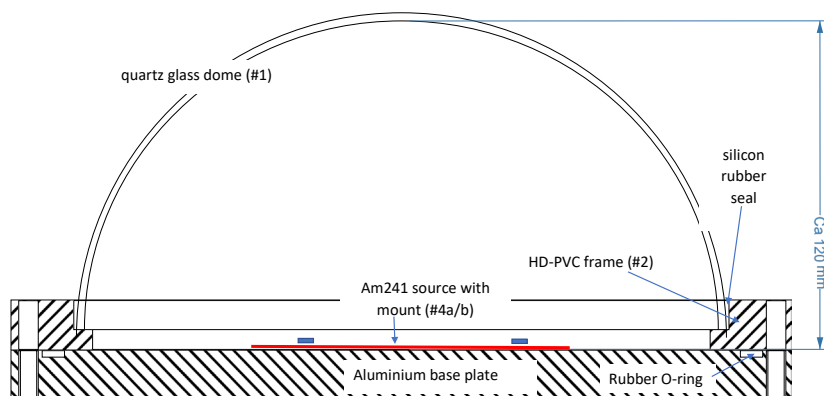be evacuated to approximately 1 hPa and purged with gas at pressures up to 1000 hPa (environmental pressure).

Figure 9. Cross-sectional view of the americium source chamber.

From the radiological point of view, this enclosed source is considered sealed, and the only concern is the external exposure to [241]Am gamma emissions. The 12 cm-high dome, with a 5 mm-thick wall and nominal outer diameter of 20 cm, provided a barrier to avoid the dispersion of the radioactive material in case of an incident. The ambient dose equivalent rates, $\dot{H}$*(10), measured for the 100 MBq source in contact with the dome wall, were 30 μSv h[-1] (top of the dome) and 15 μSv h[-1] (lateral position). An exclusion zone of 2 m around the sources was applied during the tests in the field to further reduce radiation doses to all personnel to the level of background ambient dose equivalent rate level (0.1 μSv h[-1]).

The LEDs and the 100 MBq [241]Am source purged with N2+NO gas mixture have been used for the test flights with the Fresnel lens detector performed in the Drone Research Laboratory (DroneLab). The left side of Figure 10 shows the way the gas was administered to the americium source, and the right side of the figure shows how the count rate increases when the source is purged.
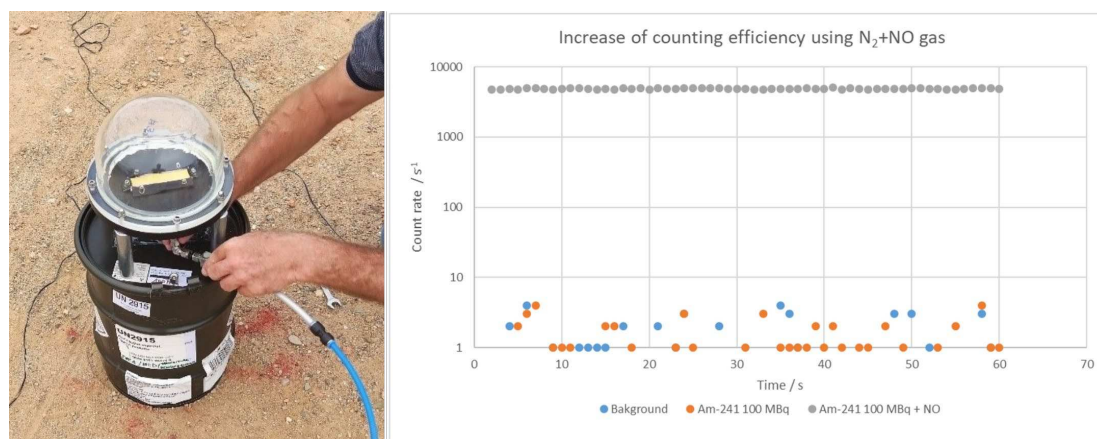

Figure 10. The N2+NO (50 ppm) gas administration to the 100 MBq [241]Am source (**left** panel) and the corresponding increase in the detector's count rate (**right** panel).

2.3. Software Architecture

The presented hardware uses a software architecture, called the RIMASpec, already used in the previous gamma detection projects [1,2]. For the RemoteALPHA project, the software was upgraded to visualize a map of alpha-emitting radionuclides in the environment in near real time.

Figure 11 illustrates the software architecture of the aerial and ground segments. The diagram displays how the software services cooperate to geolocate the detector measurements, record them in a CSV file, and send the data to the ground control station for display on a map. The

communication between the ground and air segments is managed by a server using the MQTT protocol [19]. The UAS operation and data visualization on the ground station are done via the developed web browser application.
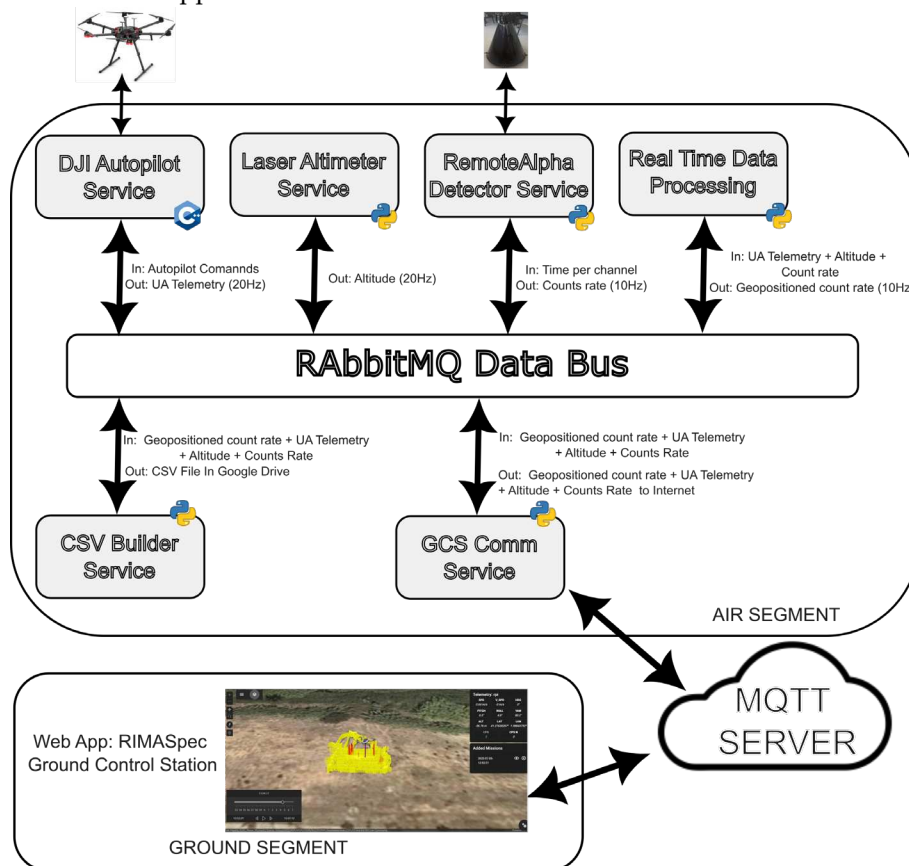

Figure 11. Air and ground software architecture schema.

2.3.1. Air Segment Software Architecture

This subsection details the operation of the air segment and the role of each service. The air segment is a distributed system where each service has a specific functionality that must be fulfilled for the whole system to work. The air segment software operates on the Raspberry Pi 4 board using the Raspberry Pi OS (previously known as Raspbian), which is the officially supported operating system.

The different services exchange information through a data bus. RabbitMQ – a message-queueing software that uses the publish/subscribe paradigm [20] – is used as a data bus. RabbitMQ facilitates the transfer of messages between connected processes: services can publish information to the bus, allowing other services interested in that information to subscribe to it.

The air segment operates as follows: the software service in charge of interacting with the UAS autopilot, called DJI Autopilot Service, publishes telemetry to the data bus at a frequency of 20Hz. At the same time, the service in charge of managing the laser altimeter, called Laser Altimeter Service, publishes the UAS altitude to the data bus with a frequency of 10Hz. Finally, the RemoteAlpha Detector Service publishes the detector's count rate every 100 ms. The Real Time Data Processing Service subscribes to all this information and merges the data. In the process, it selects the best UAS telemetry sample to geoposition the detected count rate. Once the data has been joined together, this same service publishes the geo-tagged count rate to be saved in a CSV file by the CSV Builder Service and sent to the ground control station by the GCS Comm Service using LTE (4G) network.

2.3.2. Ground Segment Software Architecture

To visualize the count rate on a map in near real time, a web application was developed. This web application has a backend and a frontend as shown in Figure 12. The backend has been developed using the Apache Tomcat Server (https://tomcat.apache.org/). Apache Tomcat is a popular open-source web server and Servlet container for Java code. For this work, this server was hosted on the same machine as the MQTT server. The backend is subscribed to the MQTT data through which all the information from the air segment arrives. The air segment information is processed and ready to be displayed on the different web browser clients (frontend). The communication between the backend and the frontend is done through web sockets and HTTP queries.
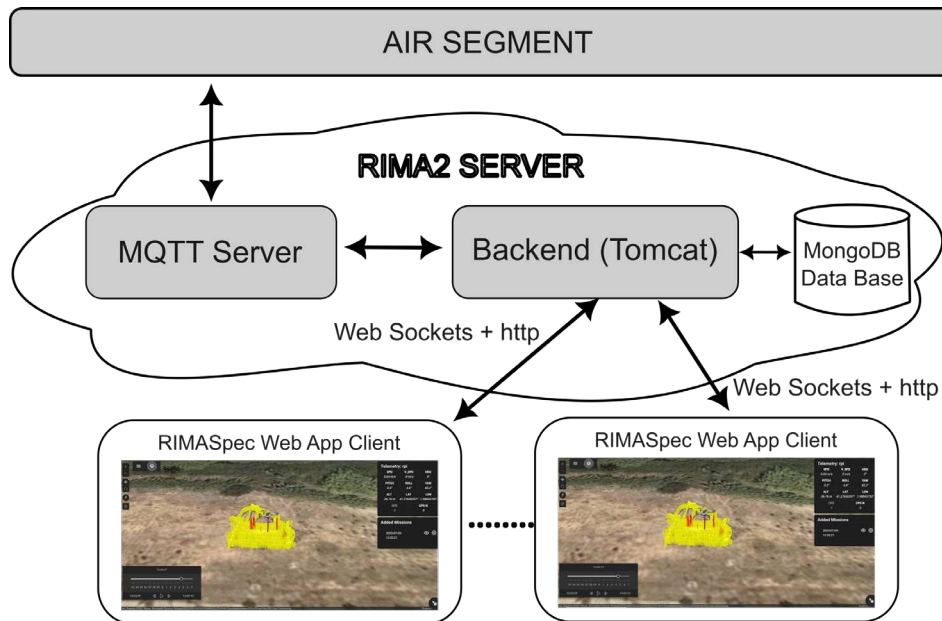

Figure 12. Software architecture of ground control station.

Web application allows any computer with an Internet connection and a browser to access the application using a username and a password requiring no additional software installation to run the RIMASpec ground control station. The web application has a database (MongoDB) where the users are created and where all the measurements with the drone are stored. The application has three user types: the administrator, the operator and the viewer. The viewer type is intended for users who are only interested in radiological information. Under the role of operator, the user has control over the UAS. The administrator can manage user profiles on top of the previously described functionality.

Once logged in, the screen shown in Figure 13 appears with three panels representing application options.
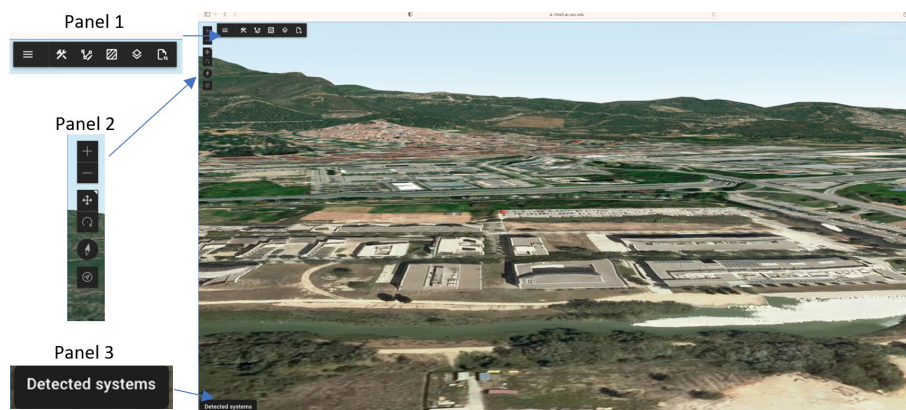

Figure 13. Ground control station web application control tab.

Panel 1 has the tools needed to create and edit a flight plan for the UAS. Through this panel, the user can create or edit an operation area and save it in a file. Then, the software can generate a flight plan over that area: for example, a random flight plan, or a flight plan with different parallel tracks. Some of these flight plans are shown in Section 3. Panel 2 presents the tools to work with the map. This panel allows zooming in and out on the map or centering the map at the UAS location. Finally, Panel 3 alerts the user when it detects a UAS that wants to connect to RIMASpec.

As mentioned above, all flight and detector data are stored in the database, and RIMASpec can replay previous flights as shown in Figure 14 which displays a screenshot of a flight performed in December 2022. The color and height of the cylinders indicate the counts measured in 0.1 seconds. The color range and height of the cylinders can be modified to optimize the visualization of the source detection. The detected counts can be also read numerically in the right-hand data box. In this data box, the UAS telemetry is also displayed: speed, pitch, roll, yaw, longitude, latitude, and altitude. Behind the telemetry box, the commands box is placed which contains the dialog for each possible command that can be sent to the UAS. The visualization software also shows the UAS position and the location on the ground where the detector is pointed (violet line). In addition, the UAS path can also be shown on the map but hidden in Figure 14 to better see the count rate markers.

RIMASpec software has more extensive functionality beyond the application-related features shown here, such as user management tools, layer visualization, and flight plan editing.
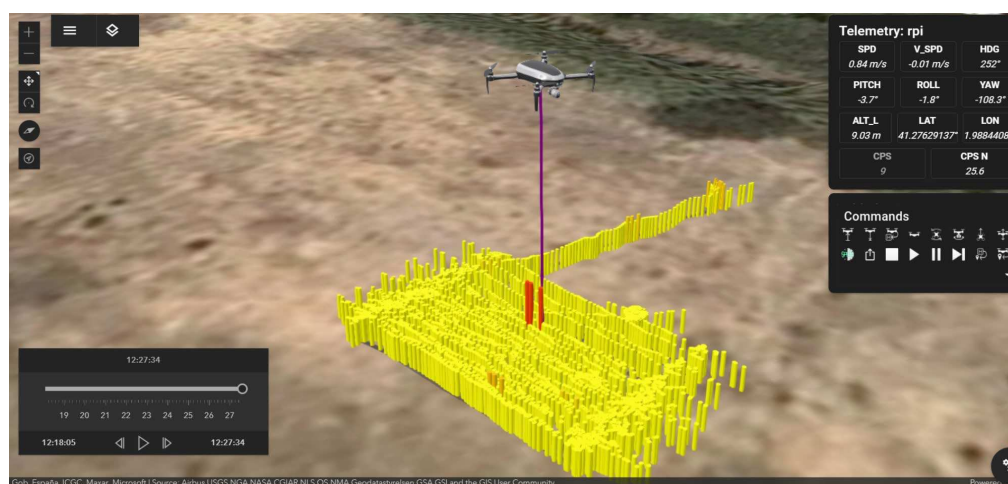

Figure 14. Screenshot of ground control station during a test flight.

3. Results and Discussion

Before performing the flights with the developed sources (LED and [241]Am) the Fresnel lens detector had to be calibrated in terms of the counting efficiency and the field of view. This was necessary since both these parameters are crucial to designing the optimum flight plans to localize the alpha sources.

3.1. Focus Configuration and the Field of View

The measurement setup illustrated in Figure 3 has been used to obtain the optimal focus configuration, the detector FOV, and the efficiency. The LED source was placed at a distance *d* ranging from 2 to 5 meters from the Fresnel lens. The PMT position *F* defines the detector protrusion from the frame (see Figure 3) which is easily measured with a ruler and represents the focal length according to the formula:

$$F = f - 40.2 \text{ cm} \tag{2}$$

The position *F* was varied in the range from 1 cm to 10 cm during the tests. The results of the count rates measured at constant LED power simulating 7.3 GBq are shown in Figure 15 with the measured most effective detector position marked with a red circle.
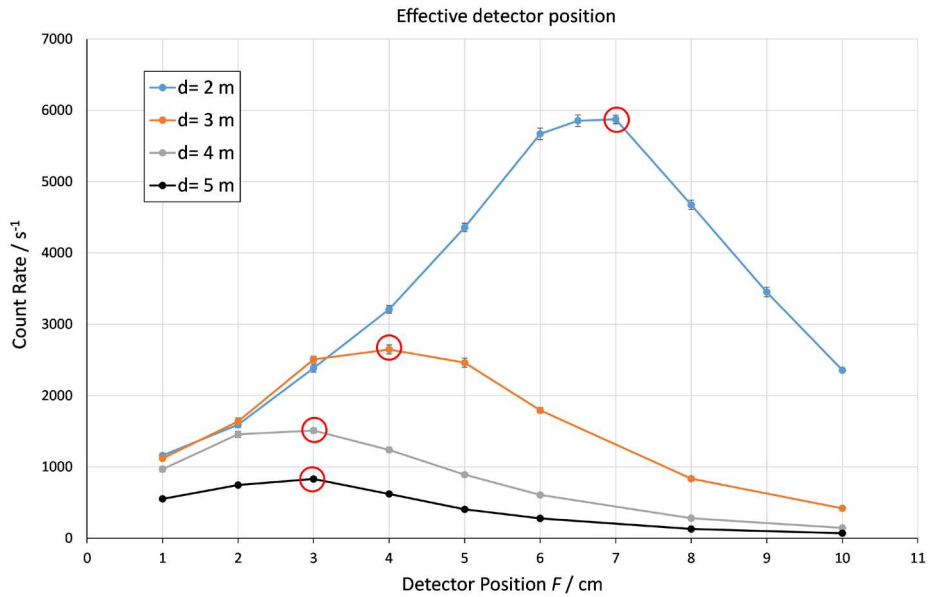
Figure 15. Count rate measured at different source-lens distances and different focus configurations F. Uncertainties in the figure correspond to standard deviations given with a 68% confidence interval (k = 1) and are attributed to the counting statistics of the detection system.

Figure 15 shows the influence of the detector position F on the detected counts for a point source located at the optical axis of the lens. At a distance of 2 m, the detector measures approximately 6000 s^{-1} at the optimal position between 6 and 7 cm; at a distance of 3 m, the count rate drops to 2500 s^{-1}, and F is between 3 and 5 cm. At larger distances, the optical detector position F is approximately 3 cm. The maximum count rate at a 5 m distance is around 800 s^{-1}. The dimensions of the laboratory did not allow testing longer distances.

Figure 16 shows the count rates measured for every lateral position h (perpendicular to the optical axis shown in Figure 3) of the LED source used to calculate the FOV and AFOV of the system at different distances to the source and focus configurations F. These parameters were estimated from the Gaussian fits of corresponding lateral profiles (see Table 2). From Table 2 it is apparent that FOV is relatively small: for a distance of 5 m and a focus configuration at 3 cm, the FOV is 10.7 centimeters.
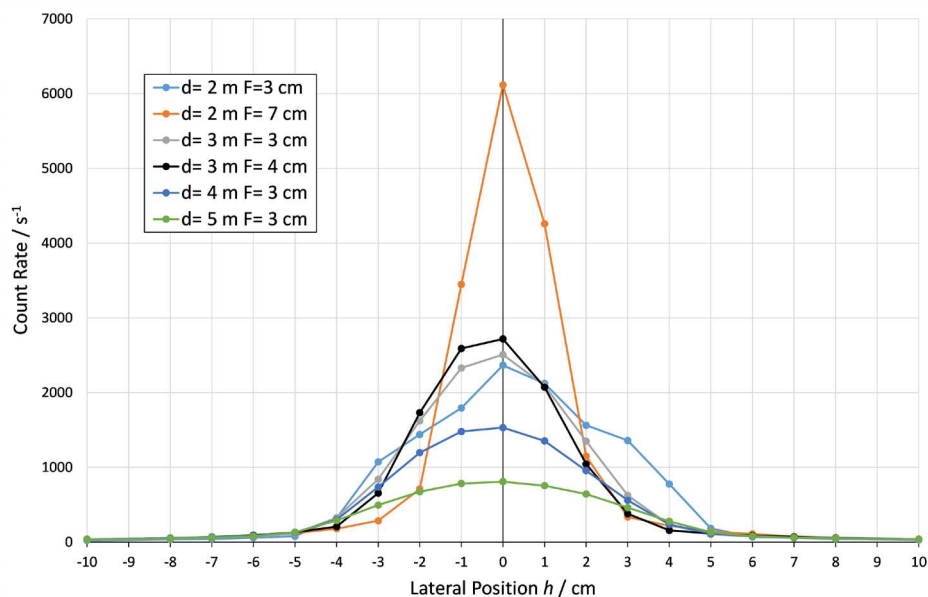
Figure 16. Count rates measured at different source-lens distances and lateral positions from the optical axis.

Table 2. Field of view and angular field of view estimated for different F positions and source-lens distances.

F (cm)	d (m)	n (s^{-1})	FOV (cm)	AFOV (°)
3	2	2240	9.6	2.75
3	3	2510	7.5	1.44
3*	4	1550	8.6	1.24
3*	5	811	**10.7**	1.22
7*	2	6070	4.1	1.17
4*	3	2770	6.4	1.23

* Indicates case for F of maximum measured count rate.

For the scenario where there are point alpha sources, the flight plan tracks should be very close together, the speed of the UAS should be very low, and the integration time should be short to maximize the probability of detecting them. Another concern with this type of scenario is that the UAS is not always completely perpendicular to the ground due to variations in wind and UAS speed resulting in changes in the roll and pitch of the whole flying system. These variations in the roll and pitch of the UAS reduce the number of counts acquired compared to a vertical position that is completely aligned with the ground. On the other hand, this variation in roll and pitch increases the probability of detecting the source because the area covered by the detector is larger than when the UAS is in constant vertical alignment.

In the case of an extended source, the detection efficiency can be obtained by laboratory calibration. In this case, the uncertainties of the detector pointing vector are not significant for the source detection and the activity calculation. In such scenarios, the detection count rate per unit activity, i.e., efficiency ε, given in units of s^{-1} MBq^{-1}, and the FOV are used to calculate the detection efficiency per unit area ε_s given in units of s^{-1} MBq^{-1} cm²:

$$\varepsilon_s = \ \varepsilon\,\pi\,\left(\frac{\text{FOV}}{2}\right)^2 \qquad (3)$$

Tables 3 and 4 list the detection efficiencies and corresponding source activities calculated according to the Table 2 data for an extended source. With relative uncertainties of the LED source and FOV of 10%, the estimated uncertainty for ε_s is about 22% [21].

Table 3. Estimation of the detection efficiency in case of an extended source with a maximum field of view focus configuration of F = 3 cm.

F (cm)	d (m)	n (s^{-1})	FOV (cm)	AFOV (°)	ε (s^{-1} MBq^{-1})	ε_s (s^{-1} MBq^{-1} cm²)
3	2	2240	9.6	2.75	0.31	22
3	3	2510	7.5	1.44	0.34	15
3	4	1550	8.6	1.24	0.21	12
3	5	811	10.7	1.22	0.11	10

Table 4. Estimation of the detection efficiency in case of an extended source with a maximum count rate focus configuration.

F (cm)	d (m)	n (s^{-1})	FOV (cm)	AFOV (°)	ε (s^{-1} MBq^{-1})	ε_s (s^{-1} MBq^{-1} cm²)
7	2	6070	4.1	1.17	0.83	11
4	3	2770	6.4	1.23	0.38	12
3	4	1550	8.6	1.24	0.21	12
3	5	811	10.7	1.22	0.11	10

Figure 17 juxtaposes the efficiency per unit area for F= 3 cm and F = MAX focus configurations at different source-lens distances. The reduction in the detection efficiency per unit area can be clearly

seen for the *F* = MAX case: while the count rate is maximized due to the tighter focus, the FOV is reduced, resulting in a lower count rate per unit area compared to the focus configuration maximizing FOV (*F* = 3 cm).
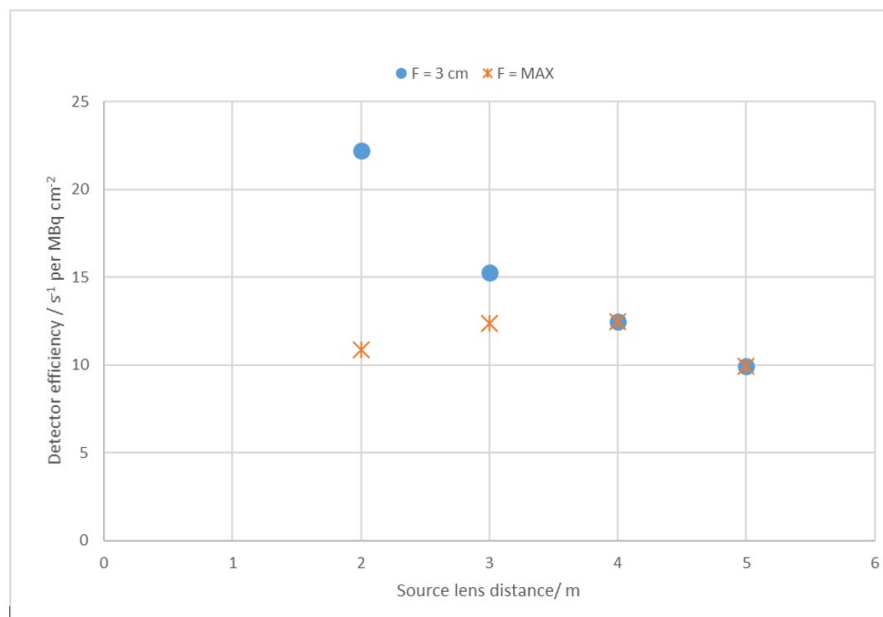

Figure 17. Comparison of the detection efficiency per unit area for different focus configurations F.

Finally, the decision threshold has been calculated to decide whether there is a significant count rate increase that indicates the presence of an alpha source. Following the ISO11929-4, the decision threshold a^*, with a 95 % confidence level, is calculated with the following equation:

$$a^* = 1.645 \cdot \tilde{u}(0) \tag{4}$$

where $\tilde{u}(0)$ is the standard deviation of background measurements.

During the flights with high solar irradiance, typical of the Spanish region, the mean and standard deviation of the UV-C background measured with the Fresnel system is around 26 ± 28 s^{-1} for an integration time of 0.1 s. Therefore, the decision threshold to identify a possible alpha source is about 46 s^{-1}. This net count rate represents a surface activity decision threshold of about 4.6 MBq cm^{-2} for integration times of 0.1 s. The 100 MBq ^{241}Am source with a 20 cm^2 active area has an activity per unit of area of 5 MBq cm^{-2}, which is too close to the decision threshold. Therefore, in order to detect the americium source, the radioluminescence intensity had to be amplified. This has been done by purging the quartz dome enclosure with N2 and 50 ppm NO gas mixture.

3.2. Optimum Flight Plans for Localization and Mapping of Alpha Emitters

Following the choice of the optimum height of 5 m elaborated in the previous section, another crucial flight plan parameter, the flight speed, is considered. The flight speed is primarily determined by the field of view of the detector. With the FOV of about 10 cm, the measurement time of 100 ms necessitates flying at a speed of 1 m s^{-1}.

The flight planner software module of the RIMASpec ground control station can generate flight plans for a UAS that cover an area with different patterns such as back and forth (Figure 18a), random, and random with genetic algorithm (Figure 18b).
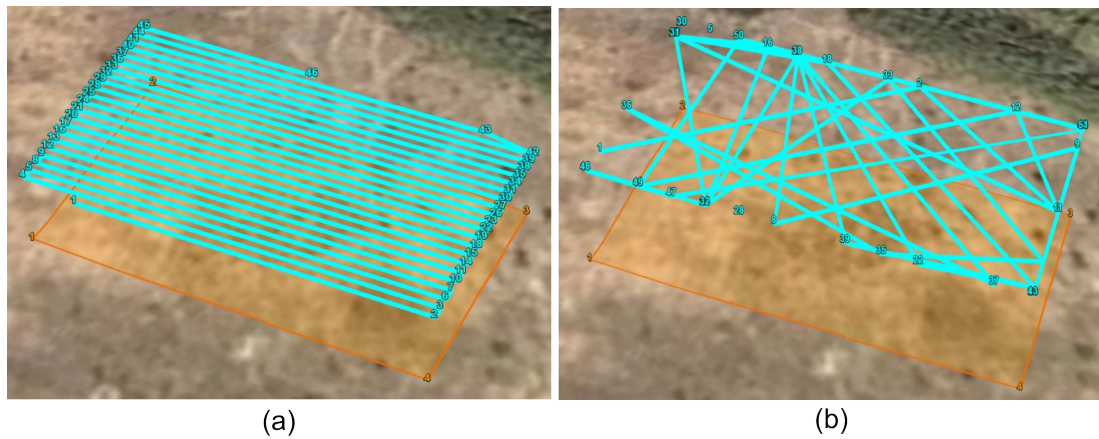
(a)   (b)

Figure 18. Examples of the scan patterns that can be generated by the ground control station.

For the test flights, a back-and-forth scan pattern was chosen to cover the whole area and to have a certain repeatability in the flight execution that the random algorithm does not offer. To cover the complete area, a distance between parallel lines of 10 cm needs to be used. However, the UAS does not permit placing waypoints in such close proximity, therefore the shortest distance allowed by the UAS, approximately 70 cm, was selected. Given the manufacturer-specified horizontal positioning error of 1.5 m, it will be necessary to perform several iterations of the parallel line scan pattern with a small offset to ensure that the UAS passes through areas it omitted in the previous iteration. The upper panels in Figure 19 illustrate the scheme of two flight plans while the bottom panels show real flights conducted according to this idea.
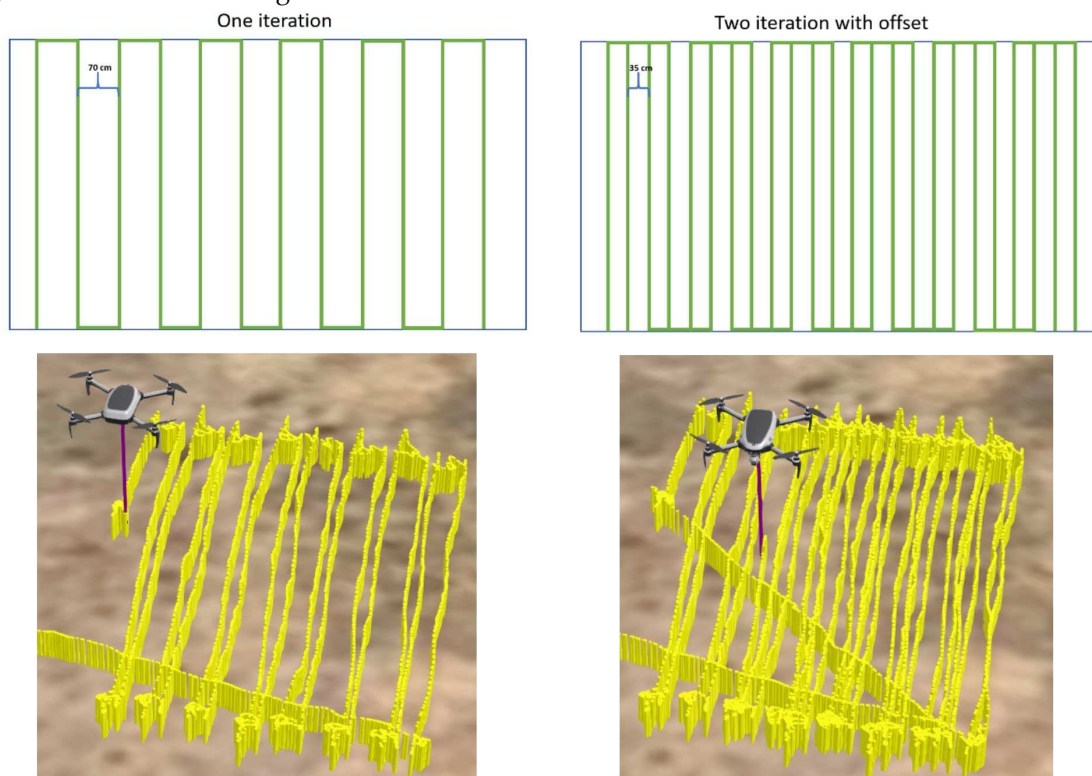

Figure 19. One iteration of the unmanned aircraft systems flight plan (**left** panel) followed by the second iteration of the flight plan with offset (**right** panel).

Each cylinder in Figure 19 corresponds to a measurement made by the detector. The markers are placed where the measurement was taken, meaning the projection is made towards the ground, taking into account the roll and pitch of the UAS. Figure 19 demonstrates how the measurements are accumulated at the ends of the flight plan tracks where the UAS decelerates, stops, and changes its

course to continue the path. It can also be observed that the decelerating before the turn causes the UAS to perform measurements outside the flight plan due to the pitch change of the UAS. In the different lines of the flight plan, due to the small variation of roll and pitch and the wind effects, the measurements are not completely aligned with the flight plan as mentioned before. These variations in roll and pitch, together with the GPS errors, make it very difficult to ensure that by following or repeating the flight plan the whole area will be scanned.

This effect can be seen even more clearly when comparing a real flight with a flight performed with the manufacturer's simulator. Figure 20 demonstrates the real and simulated flights side by side: in a simulation, the measurements are perfectly aligned.
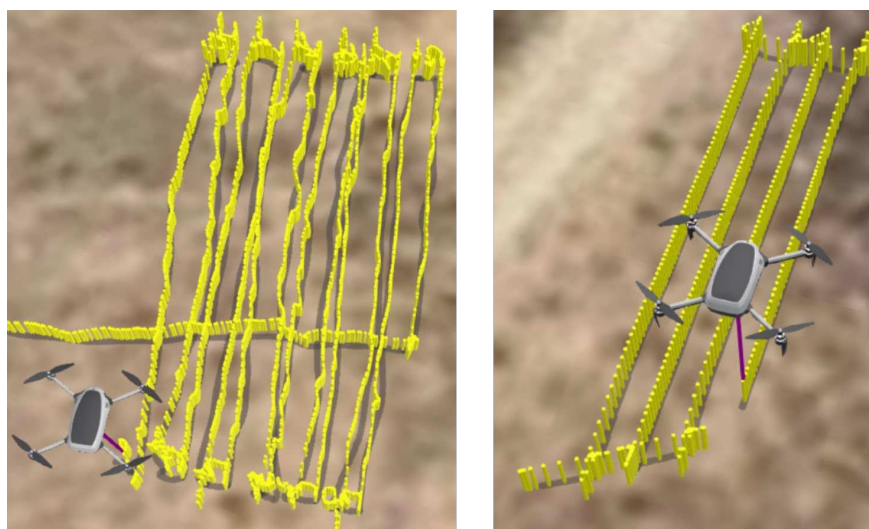

Figure 20. Comparison of a real flight (left panel) with a simulated flight (right panel).

Considering the mentioned challenges and uncertainties associated with the complete area coverage, the flights in the DroneLab were performed using the following parameters:

- Speed: 1 m s^{-1}
- Altitude above ground level: 5 m
- Distance between parallel lines: 70 cm
- Detector integration time: 0.1 s.
- Scan pattern type: back and forth
- If the sources are not detected in the first iteration of the flight plan, a second iteration with an offset will be performed.

3.3. Defining and Preparing the Flight Area

The flights were carried out at the UPC's Drone Research Laboratory (DroneLab), located in north-eastern Spain. The DroneLab is a research laboratory in the field of UAS that provides the infrastructure to carry out test flights, validation, and training for any kind of professional or research application based on UAS. The infrastructure has an $80 \times 45 \times 15 \text{ m}^3$ area, which is secure and separate from the general airspace, covered by a protective net that guarantees safety. The DroneLab allows flying in a controlled environment without the need for authorization from the authorities, despite being in an urban environment and close to the Barcelona city airport.

Figure 21 shows the flight setup with the LEDs placement and the take-off/landing area that has been used in the different test flights during the project. The landing pad made of artificial grass protects the lens from any potential damage (e.g., *dust* particles) during the landing and takeoff.

Figure 21. Typical configuration used for test flights with LED sources at the technical university of catalonia DroneLab.

3.4. Flight Test with LEDs and [241]Am Source

As mentioned before, due to GPS uncertainties and the wind effects (roll and pitch variations), the same flight plan repeated many times does not cause UAS to fly exactly over the same place and, therefore, the measurements are scattered between consecutive runs. Without this repeatability, it is very difficult to obtain the uncertainty of the source location of the point sources.

For instance, during experiments with five LEDs placed in random positions, not all of them were detected during the same iteration. During the first flight, three of the five LEDs were detected. Using the same flight plan in the following flights, either no LEDs or all of them were detected. Concluding the flight results, the probability of detecting a point source constitutes approximately 60%. This probability can be boosted by increasing the field of view of the detection system. However, increasing the FOV also has some other consequences such as the reduction of the detector efficiency and background light leakage. Extended sources with larger lateral dimensions (e.g., on the order of GPS uncertainty), on the other hand, would not be susceptible to difficulties encountered in the case of point sources.

Figure 22 shows a flight example with 5 LEDs surrounding the americium source in the middle. In a single flight plan execution, the measurement system was able to detect the americium source and 4 out of 5 LEDs. In the figure, the colormap is set such as the yellow color (background) is set to 20 s^{-1} and the red color shows the count rate of 50 s^{-1} or more, with intermediate count rate values having a color between yellow and red.
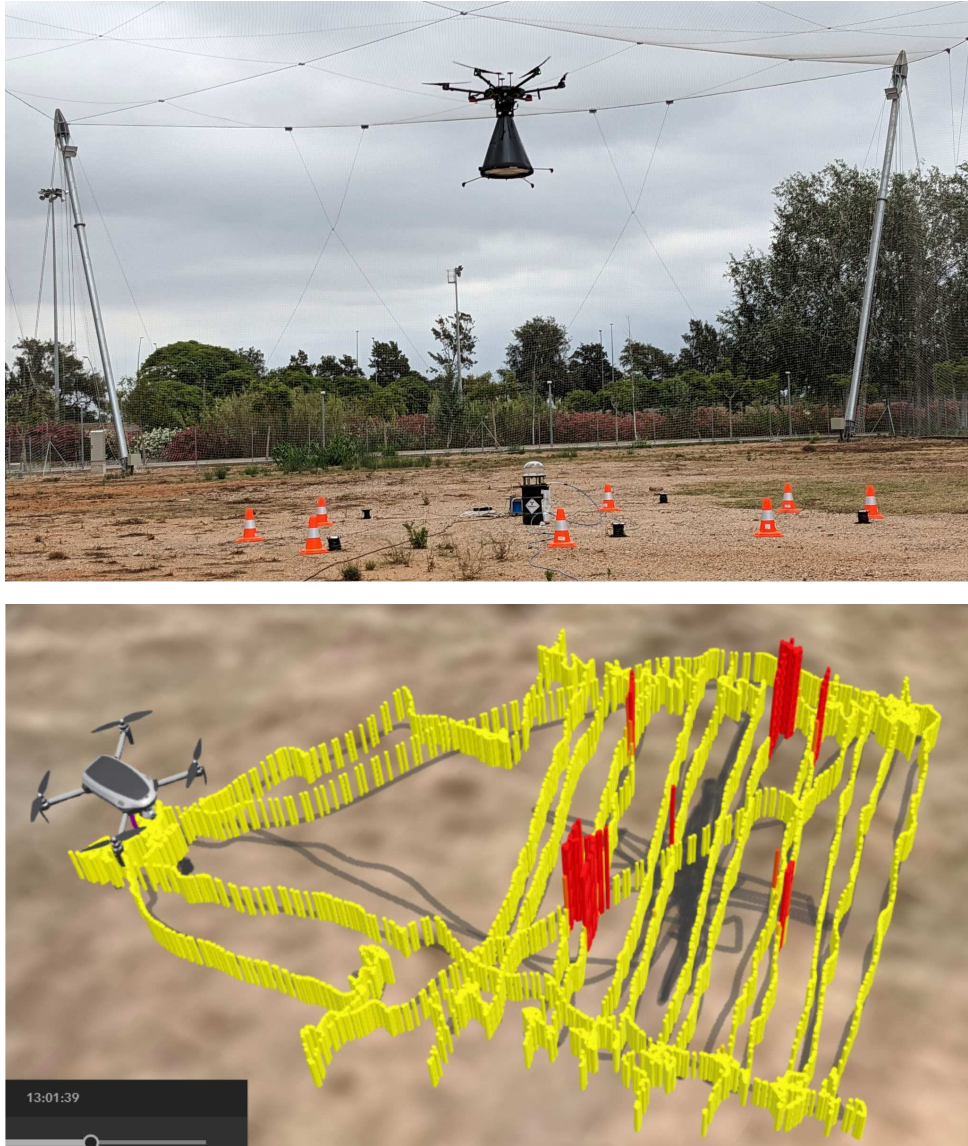
Figure 22. Flight performed with 5 LEDs and an americium source.

4. Conclusions

The main conclusion from the results presented in this manuscript is that alpha particles can be detected remotely from an unmanned aircraft system (UAS) by using optical detectors. To the extent of the authors' knowledge, this manifests the first time that alpha particles have been remotely detected from a UAS. The described prototype system, with certain operational improvements, can be used to assess contaminated areas without the need to put first responders at risk.

Another important conclusion of this work is that the operational experience gathered with the novel radioluminescence detection system can be readily applied to the extended alpha source detection (spread over the area), while the point source localization needs further hardware improvements. All test flights carried out during this study were performed using point sources – LEDs or the americium source – due to the difficulty of reproducing an extended source. Even though point sources are difficult to detect given the optical constraints, the prototype system was able to detect them with a reasonable probability of about 60%. Extended sources are far less dependent on alignment stability and are therefore much easier to detect.

Based on the results obtained in this study and in the framework of the project RemoteALPHA, it can be observed that:

- The Fresnel-lens detection system used to measure the alpha-induced radioluminescence was relatively large. This is because maximizing radioluminescence throughput while minimizing background signal requires a compromise between the diameter of the receiving optics (which determines the geometric efficiency of the system) and the focal length (which determines the FOV, that subsequently affects both the number of detected photons and filtering [12]).
- The detector's size makes the drone integration difficult which means it can only be integrated into medium- and large-sized UASs, with the sensor itself acting as a landing gear. The lens, located at the aircraft's underbelly deep below its center of gravity, resists UAS movement. Flight tests conducted in windy conditions revealed significant instabilities in UAS flight. It is not advisable to exchange the landing gear supplied by the manufacturers for incorporating the detector. Therefore, in future iterations, the compact detector design must be implemented.

The major limiting factor of the developed detection system towards the localization of point sources is its small field of view. Since the FOV of the detection system (up to 10 cm) is smaller than the uncertainty of the UAS GPS (about a meter), the detection of point sources becomes more difficult. To mitigate this issue, two clear operational improvements are therefore proposed: i) Equipping the UAS with RTK to achieve centimeter-level navigation accuracy. Results show that when the system identifies a point source during different flights, the ground station positions it at nearby locations, but not at the same location. This may be due to the GPS position uncertainties themselves. That is, with the current system we can affirm that there is alpha activity over that area, but not the exact location and how many point sources there are. With an RTK-ready UAS, the enhanced navigation would allow repeating the same flight plan: this would make passes and identify source positions more consistently and would allow estimation of the uncertainties related to the source localization; ii) Increase the FOV of the detector. This would require enlarging the PMT surface, reducing the focal length of the objective, or using mirrors with shorter focal lengths. However, this option would require a tradeoff with background light leakage [12]. An improved FOV would open the possibility of increasing the speed of the UAS and the distance between flight tracks, thus increasing the size of the area scanned with a single flight.

References

1. Royo, P. Pastor, E. Macias, M. Cuadrado, R. Barrado, C. Vargas, A. An Unmanned Aircraft System to Detect a Radiological Point Source Using RIMA Software Architecture. Remote Sensing. 10(11), 1712, (2018). https://doi.org/10.3390/rs10111712.
2. Vargas, A. Costa, D. Macia Lopez, M. Royo, P. Pastor, E. Luchkov, M. Neumaier, S., Stöhlker, U. Luff, R. Comparison of airborne radiation detectors carried by rotary-wing unmanned aerial systems. Radiation measurements, 145, 1-12 (2021). https://doi.org/10.1016/j.radmeas.2021.106595.
3. Podgorsak, E.B. Radiation Physics for Medical Physicists, Springer, 2006. https://cds.cern.ch/record/840186/files/3540250417_TOC.pdf.
4. L.A. Burchfield. Radiation Safety: Protection and Management for Homeland Security and Emergency Response. John Wiley & Sons, 2009.
5. Baschenko, S. M. Remote optical detection of alpha particle sources J. Radiol. Prot. 24 75–82, (2004).. https://doi.org/10.1088/0952-4746/24/1/006.
6. J. Sand, S. Ihantola, K. Peräjärvi, H. Toivonen and J. Toivonen. Radioluminiscence yield of alpha particles in air. New Journal of Physics 16, (2014). https://doi.org/10.1088/1367-2630/16/5/053022.

7. Sand, J. Alpha Radiation Detection via Radioluminescence of Air. PhD thesis (Tampere University of Technology. Publication; Vol. 1449). Tampere University of Technology (2016) ISBN 978-952-15-3882-7 (printed); ISBN 978-952-15-3889-6 (PDF); ISSN 1459-2045. http://www.tut.fi/tutcris.

8. Kerst, T. and Toivonen, J. Intense radioluminescence of NO/N2-mixture in solar blind spectral region. Opt Express 26, 33764-33771 (2018). https://doi.org/10.1364/OE.26.033764.

9. Faton S. Krasniqi, Thomas Kerst, Martti Leino, Jens-Tarek Eisheh, Harri Toivonen, Annette Röttger and Juha Toivonen. Standoff UV-C imaging of alpha particle emitters. Nuclear Inst. and Methods in Physics Research, A 987 (2021). https://doi.org/10.1016/j.nima.2020.164821.

10. Remote and real-time optical detection of alpha-emitting radionuclides in the environment (RemoteALPHA) project official web-site. Available online: https://remotealpha.drmr.nipne.ro/ (accessed 30 August 2023).

11. Parc Mediterrani de la Tecnologia, DRONELAB Section. Available online: https://pmt.es/ca/dronlab (accessed 30 August 2023).

12. Luchkov M, Dangendorf V, Giesen U, Langner F, Olaru C, Zadehrafi M, Klose A, Kalmankoski K, Sand J, Ihantola S, Toivonen H, Walther C, Röttger S, Ioan MR, Toivonen J, Krasniqi F (2023) Novel optical technologies for emergency preparedness and response: Mapping contaminations with alpha-emitting radionuclides. Nucl. Inst. Meth. A 1047:167895.

13. Hamamatsu Photonics web-site; Photon counting head PMT modules Section. Available online: https://www.hamamatsu.com/us/en/product/optical-sensors/pmt/pmt-module/photon-counting-head/H11870-09.html (accessed 30 August 2023).

14. GBS Elektronik GmbH web site, Multi-Channel Analyzer Section. Available online: https://www.gbs-elektronik.de/en/nuclear-measurements/multi-channel-analyzer.php (accessed 30 August 2023).

15. LightWare Lidar LLC web-site. Available online: https://lightwarelidar.com/products/sf11-c-100-m (accessed 30 August 2023).

16. Raspberry Pi official website. Available online: https://www.raspberrypi.com/products/raspberry-pi-4-model-b/ (accessed 30 August 2023).

17. Sixfab official website. Available online: https://sixfab.com/product/raspberry-pi-4g-lte-modem-kit/ (accessed 30 August 2023).

18. Table of Radionuclides (Vol. 5 – A = 22 to 244). M.-M. Bé et al. 2010, BUREAU INTERNATIONAL DES POIDS ET MESURES. ISBN-13 978-92-822-2234-8.

19. MQTT official website. Available online: https://mqtt.org/ (accessed 31 August 2023).

20. Available online: https://www.rabbitmq.com/ (accessed 31 August 2023).

21. European Accreditation. EA-4/02 M: 2013 Evaluation of the Uncertainty of Measurement in Calibration. 2013, p. 75. Available online: https://www.twirpx.com/file/1996254/ .